CHEMISTRY OF MATERIALS

ARTICLE

pubs.acs.org/cm

pH-Promoted Exponential Layer-by-Layer Assembly of Bicomponent Polyelectrolyte/Nanoparticle Multilayers

Chunqing Peng,[†] Yonathan S. Thio,[†] Rosario A. Gerhardt,[*,†] Haile Ambaye,[‡] and Valeria Lauter[‡]

[†]School of Materials Science and Engineering, Georgia Institute of Technology, Atlanta, Georgia 30332, United States

[‡]Spallation Neutron Source, Oak Ridge National Laboratory, Oak Ridge, Tennessee 37831, United States

Supporting Information

ABSTRACT: Exponential growth of layer-by-layer (LbL) assembled films is desirable because this method considerably increases the growth rate, resulting in much thicker films in a shorter period of time than is the case with normally linearly grown LbL thin films. For the first time, we demonstrate the exponential LbL (e-LbL) growth of poly(ethyleneimine)/SiO_2 nanoparticles (PEI/SiO_2) bicomponent thin films that consist mostly of SiO_2 nanoparticles (over 90 wt % obtained by thermogravimetric analysis). These results are in contrast to earlier e-LbL studies, where the film thickness was made up mostly of the polyelectrolyte, with a very small percentage coming from the inorganic nanoparticles. Here, we show that the LbL growth of the PEI/SiO_2 system significantly depends on the pH of the PEI and the SiO_2 solutions. The e-LbL growth will only occur when the film is deposited with PEI at a high pH and SiO_2 at a low pH. The exponential growth was characterized using a quartz crystal microbalance, atomic force microscopy and scanning electron microscopy imaging, and neutron reflectometry. It is demonstrated that e-LbL films can grow to thicknesses as large as 2−3 μm within just 10 bilayers. The findings reported in this article emphasize new opportunities for the e-LbL growth of organic/inorganic bicomponent composite thin films that may have applications as electrically conducting films, hydrophobic films, and brick-and-mortar biomimetic films.

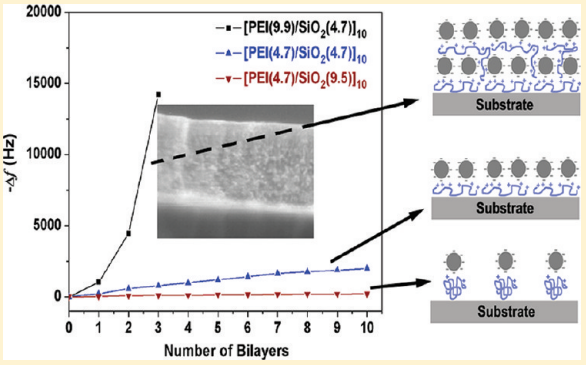

KEYWORDS: exponential growth, layer-by-layer assembly, pH-controlled assembly, polyelectrolyte/nanoparticle bicomponent thin films

INTRODUCTION

In the past two decades, layer-by-layer (LbL) assembly has become a very promising technique for fabricating multifunctional nanocomposite thin films.[1−11] Using this technique, composite thin films can be prepared by repeatedly exposing a substrate to two or more component materials, which usually contain opposite electric charges. LbL has experienced fast growth thanks to its versatility, simplicity, and robustness. A vast majority of functional thin films and coatings have been demonstrated by LbL assembly of oppositely charged species, including polyelectrolytes, inorganic nanomaterials, DNA, proteins, and viruses.[12−16]

To date, two types of LbL thin films have been reported in the literature depending on the deposition mechanism: linearly grown LbL (l-LbL) films and exponentially grown LbL (e-LbL) films. Under the l-LbL growth, the thin film mass and thickness grow linearly with the number of deposition steps. The growth of l-LbL thin films has been widely observed, and the physiochemical mechanism for this process is well understood. It was discovered that the thin film mass and thickness can also grow exponentially with the number of deposition steps, and this type of LbL thin film has been called e-LbL film.[17,18] Because of its exponentially growing nature, the thin film growth rate is enhanced significantly compared to l-LbL films. In some cases, exponential growth is followed by a linear growth with a much faster deposition rate than is observed when the growth is strictly linear. The e-LbL process has been attributed to the excess number of counterions available on the thin film surface as a result of the "in-and-out" diffusion of at least one of the polyelectrolyte components.[19−23]

Since the initial reports on the e-LbL grown thin film using polylysine and alginate,[17] the research on e-LbL thin films has experienced rapid growth. Not only have polyelectrolyte components with biological nature[17,18,24,25] been shown to exponentially grow but also other polyelectrolytes that have traditionally exhibited linear growth have now been observed to undergo exponential growth under certain promoting conditions, such as ionic strength,[26] temperature,[27] and pH.[28] The e-LbL growth of polyelectrolyte multilayers promoted by the ionic strength and temperature was attributed to the enhancement of polyelectrolyte chain diffusion, which is due to the weakening of the polyelectrolyte−polyelectrolyte interactions and entropy increment.[29] Fu et al. have observed that the pH of the weak polyelectrolytes,

Received: July 5, 2011
Revised: August 30, 2011
Published: September 22, 2011

polyethyleneimine (PEI) and poly(acrylic acid) (PAA), can also be used to tune the buildup of $[PEI/PAA]_n$ multilayers from l-LbL to e-LbL growth.[28] The pH values of PEI and PAA solutions were chosen so that the charge density of the polyelectrolyte chains in solution was minimized, whereas the charge density of the outermost polyelectrolyte layer on the substrate was maximized.[26] In other words, the film surface charge will increase significantly, not only as a result of the polymer diffusion but also as a result of the increased charge density of individual chains.

Up to now, most of the e-LbL growth has been observed in polymeric or organic systems. It would be very promising to expand the e-LbL method to inorganic materials, because films grown by the LbL assembly of polyelectrolyte/inorganic nanomaterials have shown exceptional mechanical,[8,22] electrical,[30,31] optical,[9,32] and biological properties.[17,23,33] Ball et al. demonstrated the exponential growth of composite membranes using a reactive build-up approach with an inorganic precursor (the inorganic content of the film was not determined).[34,35] Podsiadlo et al. have demonstrated the exponential LbL growth of polymer/clay films by substituting every other PAA layer in the $[PEI/PAA]_n$ e-LbL system with Na^+-motmorillonite (MTM) nanosheets to prepare the $[PEI/PAA/PEI/MTM]_n$ tricomponent composite film.[36,37] When all of the PAA layers were substituted by MTM to prepare the $[PEI/MTM]_n$ bicomponent film, they found that the thin film growth rate was significantly diminished, and the growth process transferred from exponential growth to the typical slow linear growth rate.[36] In addition, even though only every other PAA layer in the $[PEI/PAA]_n$ system was substituted by MTM, less than 10 wt % of the obtained thin film was composed of inorganic nanoparticles. A similar film composition was also observed during the e-LbL assembly of a PAA−$CaCO_3$ complex and poly(allylamine hydrochloride) (PAH), in which system less than 10 wt % of the obtained films were composed of inorganic $CaCO_3$ nanofillers.[22]

A recent paper reported the preparation of an e-LbL thin film that was primarily composed of inorganic nanoparticles during the assembly of Prussian Blue, gentamicin sulfate, and chitosan;[23] however, there has yet been no report on achieving a bicomponent e-LbL film that consists mostly of inorganic nanoparticles. Such films would be highly desirable for applications that require excellent nanoparticle interconnections or where the functionality desired depends primarily on the inorganic nanoparticle properties. Examples of applications that would require these types of films include the optimization of the electrical conductivity of nanotube, graphene, or ITO solution-based films for EMI shielding, ultracapacitor energy storage applications, or transparent electrodes. Other desired multifunctional films would be conformal protective coatings for applications that require high resistance to indentation loading or fracture resistance.

The main purpose of this paper is to answer the question as to whether it is possible to assemble organic/inorganic bicomponent composite films with high inorganic content through the e-LbL method. Here, we report results on the e-LbL assembly of $[PEI/SiO_2]_n$ thin films, in which n is the number of bilayers. PEI was chosen as the polycation because of its proven diffusibility during the LbL assembly process[28,38] and its charge density variability over the pH range 2−10.[38−40] In this work, the LbL assembly process of $[PEI/SiO_2]_n$ films is studied using a quartz crystal microbalance (QCM), atomic force microscopy (AFM), scanning electron microscopy (SEM), neutron reflectometry (NR), and thermogravimetric analysis (TGA).

EXPERIMENTAL SECTIONS

Materials. Branched PEI ($M_w \sim 750\,000$ g/mol, pK_a[39] ~ 10), LUDOX AS-40 SiO_2 colloidal suspensions (particle size ~30 nm, 40 wt %), and 11-mercaptoundecanoic acid (MUA) were obtained from Sigma Aldrich. All of the materials were used as received without further purification. The LUDOX AS-40 SiO_2 colloidal suspensions were analyzed using Zetasizer (Malvern Instrument, Nano-ZS) at the pH range 2−9.5.

Layer-by-Layer Assembly. The PEI solution and the SiO_2 suspension were respectively prepared as 0.02 and 1 wt % concentrations using pure water (resistivity 18.2 MΩ·cm). The pH was adjusted to the desired value using sodium hydroxide or hydrochloric acid. No NaCl was added intentionally unless specifically mentioned. A typical sample preparation process is described as follows: the substrate was first immersed in the PEI solution for 5 min, washed with pure water, blow dried with pure nitrogen, immersed in the SiO_2 suspension for 10 min, washed with pure water, and blow dried with pure nitrogen. This procedure describes a complete assembly cycle for one bilayer, and it was repeated as many times as necessary to obtain a film with the desired number of bilayers. In this paper, we denote the thin film that was assembled in PEI solution at a pH of 9.9 and SiO_2 suspension at a pH of 4.7 for 10 bilayers as $[PEI(9.9)/SiO_2(4.7)]_{10}$.

QCM Study of the Thin Film Growth. The thin film growth process was investigated using quartz crystal microbalance (QCM, Stanford Research System, Inc., QCM 200). The quartz crystals used were AT cut crystals, coated with chrome/gold electrodes which resonate at 5 MHz at room temperature. The quartz crystals were treated using the procedure that we described elsewhere.[31] In brief, the crystals were first cleaned with piranha solution (2:1 H_2SO_4/H_2O_2) (Caution! Piranha solution is extremely reactive and exothermic, and it should be handled with extreme care) for 1 h. The cleaned crystals were then immersed into 1 mM MUA ethanol solution for over 24 h to construct a self-assembled monolayer (SAM) of MUA on the gold electrode of the crystals. The SAM-modified crystals were then treated with 1 mM NaOH solution for 3 min to render a negative surface charge on the crystal. The treated crystals were then used as the substrate to assemble $[PEI/SiO_2]_{10}$. These crystals were cleaned with pure water and blow-dried with pure nitrogen prior to the QCM measurement after every assembly step.

AFM and SEM Study of the Film Structure and Thickness. The thin film surface structure and thickness on quartz crystals after certain assembly steps were characterized using an atomic force microscope (AFM, Park Systems, XE-100E). The crystals were carefully handled, and the resonance frequency was checked before and after the AFM imaging to ensure the most accurate QCM measurement. All of the AFM images were obtained under noncontact mode in air. The AFM tips (nanosensors, NCHR) exhibit a nominal tip radius smaller than 10 nm, resonate at approximately 300 kHz, and have a spring constant around 40 N/m. The AFM images were analyzed to obtain the root-mean-squared (rms) roughness.

The thin film thickness could be evaluated by correlating the true film thickness, t, with the resonance frequency change of QCM crystals, $-\Delta f$, through a constant C_f according to the Sauerbrey equation:[41]

$$t = C_f(-\Delta f) \quad (1)$$

The true film thickness, t, can be measured by evaluating a line profile across a scratch on the film using AFM (see Figure S1 in the Supporting Information).

The cross section of the films that were deposited onto glass slides was evaluated using scanning electron microscopy (SEM, Hitachi S-800). The images were acquired at an accelerating voltage of 15 kV in backscattering imaging mode.

Neutron Reflectometry Study of the Film Structure. The thickness and structure of the films that were deposited onto silicon wafers were evaluated using neutron reflectometry (MAGICS reflectometer,

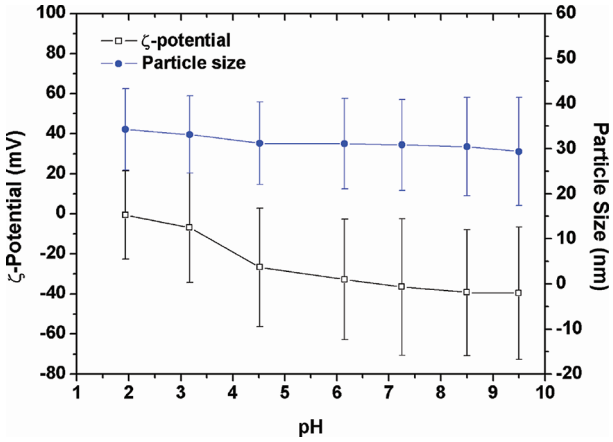

Figure 1. ζ-Potential and particle size analysis of SiO_2 colloidal suspensions.

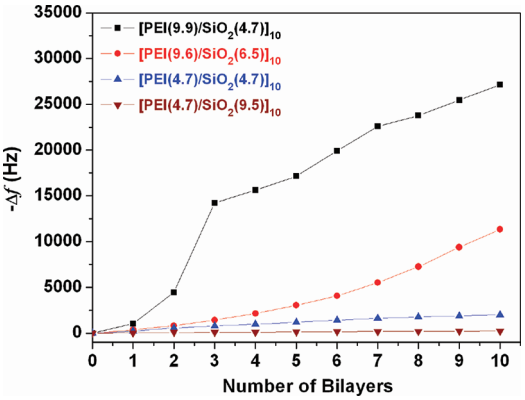

Figure 2. QCM crystal frequency change ($-\Delta f$) during LbL assembly of $[PEI(9.9)/SiO_2(4.7)]_{10}$, $[PEI(9.6)/SiO_2(6.5)]_{10}$, $[PEI(4.7)/SiO_2(4.7)]_{10}$, and $[PEI(4.7)/SiO_2(9.5)]_{10}$ thin films.

Spallation Neutron Source at Oak Ridge National Laboratories). This reflectometer is a time-of-flight (TOF) instrument with a wavelength band ranging from 2 to 4.75 Å centered at the highest intensity of the incident beam.[42,43] The experiment is performed in a grazing incidence geometry. A highly collimated neutron beam impinges on the sample surface at an angle α_i, and the intensity of the neutrons, reflected and scattered under angles α_f, is registered using a position sensitive detector, as a function of their time-of-flight from the source. For the specular reflection (i.e., $\alpha_i = \alpha_f$), the reflectivity is a function of the momentum transfer Q_z, which is a function of the incident angle α_i, the neutron wavelength λ (shown in eq 2), and the scattering length density profile (SLD).

$$Q_z = \frac{2\pi \sin \alpha_i}{\lambda} \quad (2)$$

The SLD is determined by the chemical and structural depth profile through the thickness of the film with a resolution of 0.5 nm. By simulating the reflectivity curves using the proposed scattering length density (SLD) profiles of the thin films and fitting to the experimental data, the structure information about the LbL thin films can be determined

TGA Study of the Inorganic Content of the Thin Films. The inorganic content of the thin film $[PEI(9.9)/SiO_2(4.7)]_{50}$ deposited onto a glass substrate was analyzed using TGA. The thin film samples were collected by scraping the thin film off of the glass substrates using razor blades, and the collected samples were heated to 800 °C in air, at a heating rate of 5 °C/min. The remnant material was considered to be noncombustible inorganic SiO_2.

To evaluate the actual content that was contributed by the SiO_2 nanoparticles, which includes both the noncombustible SiO_2 and the combustible stabilizing agents, we also analyzed colloidal SiO_2 nanoparticles by TGA using the same heating procedure. The colloidal SiO_2 particles were first spin-coated onto a glass substrate, and the particles on the glass substrate were then collected by scraping them off of the glass substrate, as described prior to the TGA analysis.

RESULTS AND DISCUSSION

ζ-Potential and Particle Size Analysis of SiO_2 Colloidal Suspensions. The ζ-potential and the particle size of the SiO_2 suspensions are shown in Figure 1. As shown in the figure, the SiO_2 particle size remains around 30 nm for the pH range 2−9.5. Furthermore, the ζ-potential of the SiO_2 suspension is also relatively stable around −30 mV at a pH above 4.5. Therefore, the SiO_2 colloidal suspension can be considered to be a stable suspension at pH 4.5. In this pH range, the SiO_2 nanoparticles exhibit a negative charged surface without too much charge density variation. Therefore, the PEI and SiO_2 counterion pair provides a perfect opportunity to demonstrate the pH-promoted exponential growth of LbL bicomponent polyelectrolyte/inorganic nanoparticle thin films.

QCM Study of the pH-Promoted Exponential Growth of $[PEI/SiO_2]_n$ Thin Films. Several combinations of pH values for PEI solutions and SiO_2 colloidal suspensions were chosen to study the effect of pH on the assembly process. As shown in Figure 2 and Table 1, the LbL assembly of $[PEI/SiO_2]_n$ thin films was significantly affected by the pH difference between the PEI solutions and the SiO_2 suspensions. When PEI and SiO_2 were assembled at pH 9.9 and 4.7, respectively, to prepare thin film $[PEI(9.9)/SiO_2(4.7)]_{10}$, the LbL assembly process exhibited extremely fast exponential growth in the first three bilayers and then transferred to a linear growth with a fairly fast growth rate. The growth rate in the exponential growth regime was so fast that more than 50 wt % of the 10-bilayer thin film was contributed by the first three assembly bilayers. However, when the thin film was deposited with PEI at a pH of 9.6 and SiO_2 at a pH of 6.5, the exponential growth rate of films was greatly diminished, although, in this case, the exponential process lasted until the ninth bilayer before the transition from exponential growth to linear growth occurred. As a result of the depressed exponential growth, the thin film $[PEI(9.6)/SiO_2(6.5)]_{10}$ only exhibited less than half the thickness of film $[PEI(9.9)/SiO_2(4.7)]_{10}$ (see Figure 2 and Table 1). Interestingly, the linear growth rate after the exponential-to-linear transition during the assembly of $[PEI(9.9)/SiO_2(4.7)]_{10}$ and $[PEI(9.6)/SiO_2(6.5)]_{10}$ was quite similar.

When the thin film was assembled in PEI and SiO_2 solutions at the same pH of 4.7, the LbL assembly process exhibited a typical l-LbL growth, at a much smaller growth rate. In fact, the linear growth rate of the $[PEI(4.7)/SiO_2(4.7)]_{10}$ film was 10 times slower than that of the linear growth regime during the e-LbL assembly processes (see Table 1). Furthermore, when thin films were assembled in PEI at a pH of 4.7 and in SiO_2 at a pH of 9.5, even less material was deposited after 10 bilayers. Therefore, we can conclude that the LbL assembly process will only exhibit e-LbL growth when the thin film is assembled with PEI at a high pH and with SiO_2 at a low pH. When the pH difference between PEI and SiO_2 is small or when SiO_2 is at a high pH and PEI is at a

dx.doi.org/10.1021/cm2019229 |Chem. Mater. 2011, 23, 4548–4556

Table 1. Film Thickness Calculated from QCM Results

film[a]	$-\Delta f$ at the 10th bilayers (Hz)	total thickness[b] (nm)	thickness from e-LbL growth[b] (nm)/ number of e-LbL growth steps	thickness from l-LbL growth[b] (nm)/ number of l-LbL growth steps
$[PEI(9.9)/SiO_2(4.7)]_{10}$	27130	2143	1123/3	1020/7
$[PEI(9.6)/SiO_2(6.5)]_{10}$	11345	896	741/9	155/1
$[PEI(4.7)/SiO_2(4.7)]_{10}$	2000	158	0/0	158/10
$[PEI(4.7)/SiO_2(9.5)]_{10}$	212	17	0/0	17/10

[a] To differentiate the films, the pH values of the PEI solutions and SiO_2 suspensions were chosen to be denoted in the parentheses. [b] The total thickness values were all calculated from the $-\Delta f$ value using eq 1) with the C_f constant as 0.079 nm/Hz. This constant was obtained by measuring the film thickness using AFM (see Figure S1 in the Supporting Information).

low pH, the e-LbL growth will disappear. The e-LbL film $[PEI(9.9)/SiO_2(4.7)]_{10}$ and l-LbL film $[PEI(4.7)/SiO_2(4.7)]_{10}$ showed over 13 times difference in terms of the film total final mass and thickness after the 10 bilayer deposition (see Table 1).

It should be noted that the exponential-to-linear transition has often been observed during e-LbL growth process.[27,44−46] This phenomenon was explained by the possible film restructuring during the assembly process that prevents the diffusion of polyelectrolyte throughout the whole film.[27,46] As a result of this film restructuring, the number of polyelectrolyte chains that diffuse out of the film tends to be constant, and thus, the film grows linearly. Interestingly, the linear growth rates after the exponential-to-linear transition during the assembly of $[PEI(9.9)/SiO_2(4.7)]_n$ and $[PEI(9.6)/SiO_2(6.5)]_n$ were quite similar, which indicates that these two e-LbL grown films went through a similar film restructuring process.

Besides the pH difference between the PEI solution and the SiO_2 colloidal suspension, the ionic strength and the buffer strength in the solutions are also very critical to obtaining pH-controlled e-LbL growth of $[PEI/SiO_2]_n$ films. As we discuss in the Supporting Information (Figures S2 and S3), when 0.1 M NaCl was added into the PEI solution, the assembly of $[PEI(10.1, 0.1\ M\ NaCl)/SiO_2(4.7)]_{10}$ exhibited a typical l-LbL growth, instead of e-LbL growth. This was attributed to the salt screening effect[47] of NaCl on the interaction distance between PEI and SiO_2 particles during the assembly. We have also noticed that the pH of the PEI solutions and SiO_2 suspensions will gradually change as the assembly proceeds. Adding 3 mM phosphate buffer into both the PEI and SiO_2 suspensions can not only extend the e-LbL growth regime, but it also increases the growth rate in the linear growth regime (Figures S4 and S5 in the Supporting Information). More details about the ionic strength effect and the pH buffer effect can be found in the Supporting Information.

e-LbL Growth Strength. The strength of the exponential growth can be evaluated by simulating the exponential growth curve from QCM results using the following equation:[27,29]

$$-\Delta f = f_1 \exp(\beta n) - f_2 \quad (3)$$

Using this equation, the $-\Delta f$ of QCM crystals can be fitted to the exponential growth of n bilayers through fitting parameters f_1, f_2, and β. The parameters f_1 and f_2 are the kinetic scaling factors for the thin film growth process, and they are usually equal. The parameter β is the characteristic parameter for the exponential growth strength, and it has been named the exponential growth "strength factor".[27,29] A value of β close to 0 corresponds to a linearly grown thin film, whereas a large value of β means that the thin film grows exponentially. The larger the value of β, the stronger the exponential growth effect. Values of the parameter β for $[PEI/SiO_2]_n$ films grown at different conditions, as well as some other e-LbL thin films from the literature, are listed in Table 2.

Table 2. List of the Exponential Growth Strength Factors, β, for Various Counterion Pairs

counterion pairs[a]	β	ref
$PEI(9.9)/SiO_2(4.7)$	1.09	this work
$PEI(9.6)/SiO_2(6.5)$	0.22	this work
$PEI(4.7)/SiO_2(4.7)$	9×10^{-7}	this work
$PEI(4.7)/SiO_2(9.5)$	7×10^{-7}	this work
PEI(9.0)/PAA(2.85)	0.79[b]	ref 28
PLL(7.4)/PGA(7.4)	0.31[b]	ref 20
PLL(7.3)/HA(7.3)	0.24[b]	ref 18
PLL(7.0)/PAA(7.0)	0.37 (0.81)[b,e]	ref 25
PDDA/PSS	0.38[b,c]	refs 26,27
PAH(7.4)/PGA(7.4)	0.42[b,c]	refs 29, 46, 48
PB(4.0)/GS(4.0) [d]	0.043[b]	ref 23

[a] The counterion pairs are listed as cation(pH)/anion(pH) unless specifically mentioned otherwise. [b] The strength factor, β, was not stated in the reference paper. Instead, we estimated the strength factor based on the film growth curve in the reference paper. [c] The buildup of PDDA/PSS and PAH/PGA films changed from typical linear to exponential growth when the temperature and ionic strength of the polyelectrolyte solution increased, and only the highest growth strength factor is cited here. [d] The buildup of PB/GS only exhibited e-LbL growth when they had a precursor layer $[PB/CHI]_5$. [e] Two different values were obtained from ellipsometry (0.37) and QCM (0.81) measurements. The difference was attributed to the water absorbance and film swelling.

As shown in Table 2, during the assembly of $[PEI/SiO_2]_n$, the strength factor β for the exponential growth part is highly dependent on the pH difference between PEI and SiO_2. The strength factor for film $[PEI(9.9)/SiO_2(4.7)]_n$ is as high as 1.09, while the strength factor significantly decreases when the pH difference between the PEI and SiO_2 solutions decreases. The strength factors of films made from PEI solutions that had equal or lower pH than the SiO_2 ($[PEI(4.7)/SiO_2(4.7)]$ and $[PEI(4.7)/SiO_2(9.5)]_n$) are both close to zero, and they both exhibited a typical l-LbL growth. It should be mentioned that the β value of 1.09 reported here is by far the largest value ever reported. In addition, it is also noteworthy that the strength factors β for the non-pH-promoted e-LbL films are usually around or below 0.4, as shown in Table 2.

AFM Study of the Film Surface Structure. The surface structure of the films was analyzed by AFM imaging. Parts a−d of Figure 3 show the surface structure of thin films at the $2 \times 2\ \mu m^2$ scale, under which scale individual SiO_2 particles can be clearly seen. As shown in the figure, at this scale, the rms surface roughness

dx.doi.org/10.1021/cm2019229 |Chem. Mater. 2011, 23, 4548–4556

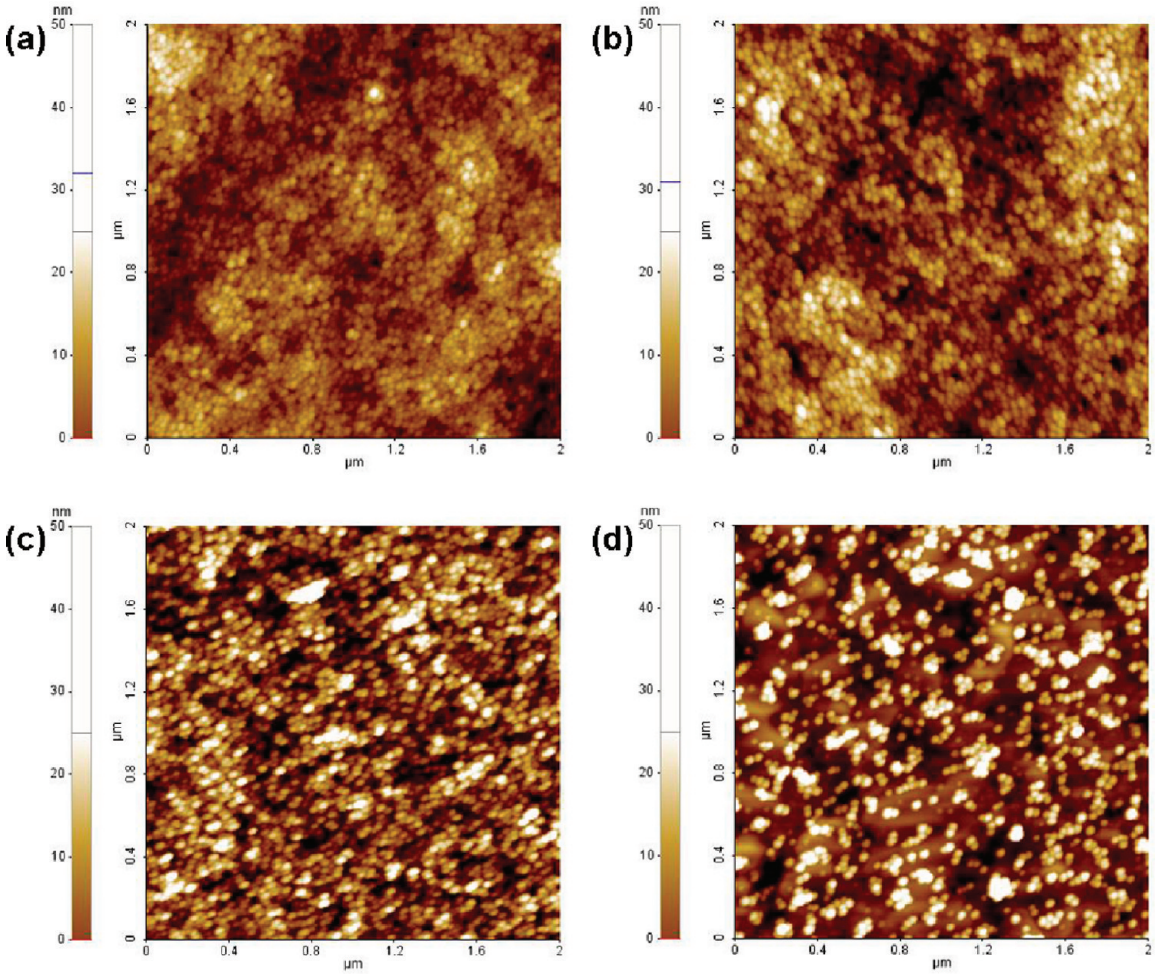

Figure 3. AFM images of films: (a) $[PEI(9.9)/SiO_2(4.7)]_{10}$, (b) $[PEI(9.6)/SiO_2(6.5)]_{10}$, (c) $[PEI(4.7)/SiO_2(4.7)]_{10}$, and (d) $[PEI(4.7)/SiO_2(9.5)]_{10}$. The rms roughness is (a) 7.3, (b) 9.3, (c) 12.5, and (d) 12.6 nm. All of the images use the same height scale for easy comparison.

of the $[PEI(9.9)/SiO_2(4.7)]_{10}$ e-LbL film is the lowest at 7.3 nm, and the rms roughness of the $[PEI(4.7)/SiO_2(4.7)]_{10}$ l-LbL film is 12.5 nm. In other words, the film surface of the e-LbL films at the $2 \times 2\ \mu m^2$ scale is smoother than that of the l-LbL films. Interestingly, as shown in Figure 3d, the $[PEI(4.7)/SiO_2(9.5)]_{10}$ thin film shows a very different film structure, where the deposited nanoparticles formed cluster-like structures, and the thin film exhibited a patchy thin film growth behavior. In addition, 10 bilayers of the thin film could not even cover the whole surface.

The surface structure of the thin films at the $30 \times 30\ \mu m^2$ scale was also analyzed, and the 3D images of the film surface structure are shown in Figure 4. As shown in Figure 4a, the $[PEI(9.9)/SiO_2(4.7)]_{10}$ e-LbL thin film exhibits a much rougher surface, with the peak-to-valley height differences as high as 100 nm and a rms roughness of 21 nm. This vast difference in the surface roughness between the $2 \times 2\ \mu m^2$ and $30 \times 30\ \mu m^2$ scales indicates that the $[PEI(9.9)/SiO_2(4.7)]_{10}$ e-LbL films exhibited a dual-scale structure. In contrast, this kind of dual-scale structure is not observed for the $[PEI(9.6)/SiO_2(6.5)]_{10}$ e-LbL film and $[PEI(4.7)/SiO_2(4.7)]_{10}$ l-LbL film (Figure 4b and c). No obvious difference in the rms surface roughness of these two films could be observed between the $2 \times 2\ \mu m^2$ and $30 \times 30\ \mu m^2$ scales. The unique dual-scale structure of the $[PEI(9.9)/SiO_2(4.7)]_{10}$ e-LbL films is most likely due to the strong in-and-out diffusion of PEI chains throughout the thin film during the assembly process. The in-and-out diffusion of the polymer chains can easily cause the uneven surface structure, giving rise to the surface roughness. The fact that the $[PEI(9.6)/SiO_2(6.5)]_{10}$ e-LbL film did not show such a structure is probably due to the relatively slow e-LbL growth that it experienced (see Figure 2 and Table 1).

It is worth noting that a similar film structure has also been observed for other e-LbL grown tricomponent films, but the increased roughness was attributed to nanoparticle clustering.[23] We think that the dual-scale nature of our films is more than just the clustering of nanoparticles, because only the fast grown e-LbL films show the dual-scale structure, and all the l-LbL grown films do not show such a feature. In addition, if it were to be just the clustering of nanoparticles, the thin film would start growing into clusterlike structures, which was not observed. In fact, quite the opposite, the e-LbL films started with a smooth surface (see AFM images for $n = 1$ to 4 bilayer $(PEI/SiO_2)_n$ films, Figure S6 in the Supporting Information) and then transferred to the dual-scale structure at the later stages of the e-LbL film growth (as shown in Figure 4a).

NR Study of the Thin Film Structure. Neutron reflectometry (NR) was used to study the details of the internal structure of $[PEI(9.9)/SiO_2(4.7)]_n$ e-LbL films. Because of the contrast of

dx.doi.org/10.1021/cm2019229 |*Chem. Mater.* 2011, 23, 4548–4556

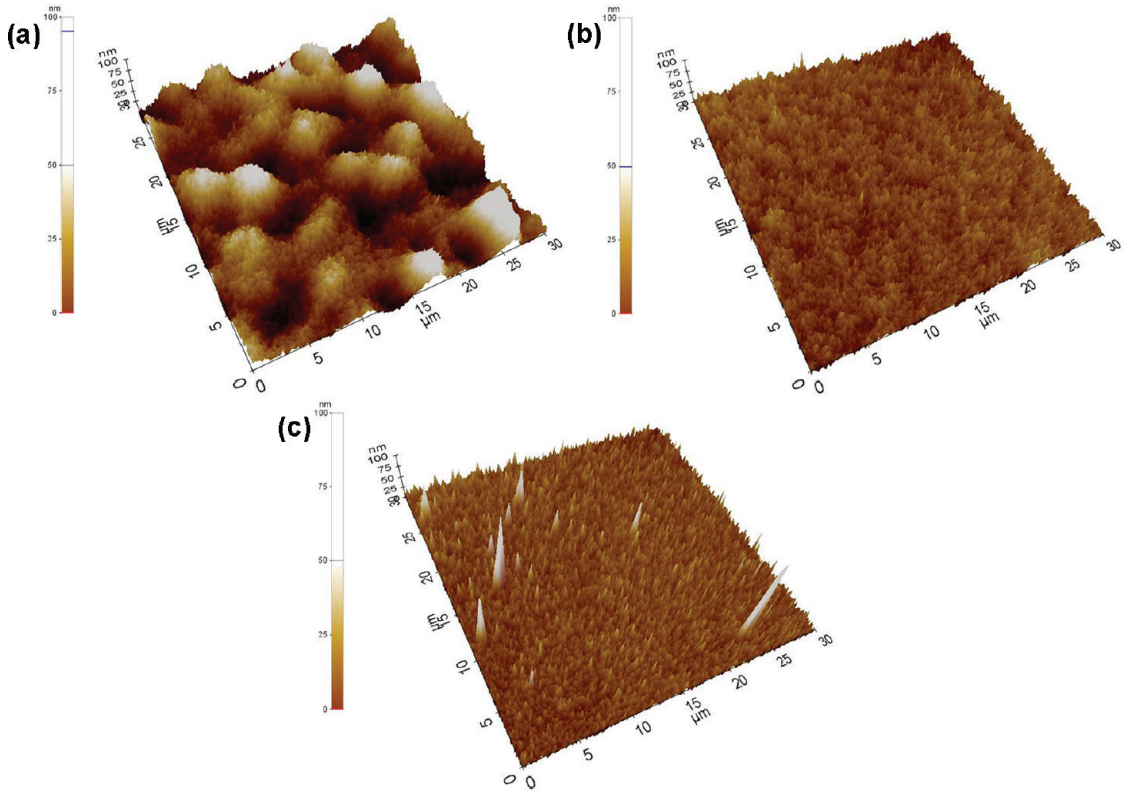

Figure 4. AFM 3D images of films: (a) $[PEI(9.9)/SiO_2(4.7)]_{10}$, (b) $[PEI(9.6)/SiO_2(6.5)]_{10}$, and (c) $[PEI(4.7)/SiO_2(4.7)]_{10}$. All of the images are a 30 μm × 30 μm scan. The *Z* scales of parts a, b, and c are kept the same for easy comparison. The rms roughness at this scale is (a) 21.5, (b) 8.1, and (c) 9.1 nm.

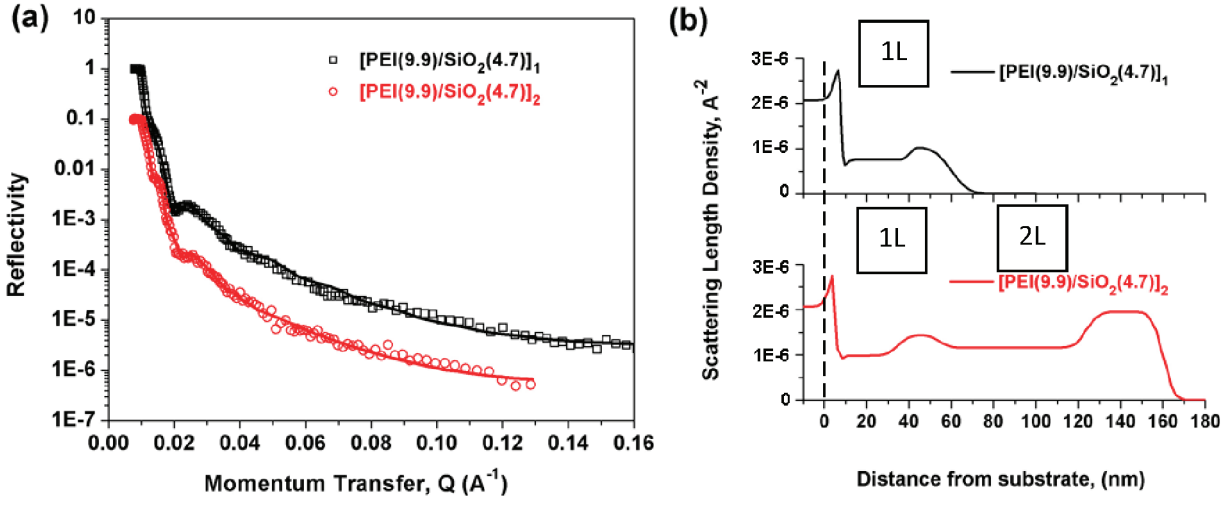

Figure 5. (a) Experimental (open symbols) and theoretical (lines) reflectivity profiles for $[PEI(9.9)/SiO_2(4.7)]_1$ and $[PEI(9.9)/SiO_2(4.7)]_2$ films deposited on silicon wafers. The curves are offset by a factor of 0.1 for clarity. (b) Neutron scattering length density profiles obtained from the simulation shown as functions of the distance from the substrate. The dashed line marks the surface of the Si substrate; the peaked intensity of the substrate corresponds to the naturally oxidized SiO_2 on the surface of the substrate, which is formed prior to film deposition. The labels 1L and 2L indicate the first and second bilayer.

scattering length density (SLD) between the PEI and the SiO_2 particles, NR provides the unique possibility to probe the details of the internal film structure through the SLD depth profile of the composite films.[49] As a result of the high depth resolution of 0.5 nm, this method allows us to study a single ($[PEI(9.9)/SiO_2(4.7)]_1$) and a double layer ($[PEI(9.9)/SiO_2(4.7)]_2$) film and gives direct access to the details of the exponential growth. The experimental reflectivity results, the fitted results, and the SLD profiles for $[PEI(9.9)/SiO_2(4.7)]_1$ and $[PEI(9.9)/SiO_2(4.7)]_2$ thin films are shown in Figure 5.

The reflectivity results, displayed in Figure 5a, were fitted well using the proposed SLD profiles shown in Figure 5b. According

dx.doi.org/10.1021/cm2019229 |*Chem. Mater.* 2011, 23, 4548–4556

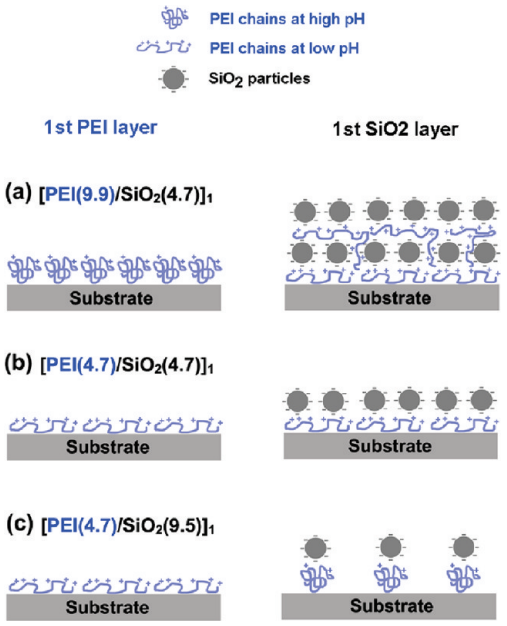

Figure 6. Schematic illustration of the first bilayer assembly structure for films: (a) $[PEI(9.9)/SiO_2(4.7)]_1$, (b) $[PEI(4.7)/SiO_2(4.7)]_1$, and (c) $[PEI(4.7)/SiO_2(9.5)]_1$. For each thin film, the assembly of the first PEI and SiO_2 layers are illustrated separately.

to Figure 5b, the SLD profile of the $[PEI(9.9)/SiO_2(4.7)]_1$ film through the film depth consists of two regions: a bottom layer with a lower SLD value ($\sim 7.6 \times 10^{-7}$ Å^{-2}) and a top layer with a higher SLD value ($\sim 1 \times 10^{-6}$ Å^{-2}). Because the SLD of SiO_2 is higher than that of PEI, this suggests that the film $[PEI(9.9)/SiO_2(4.7)]_1$ is comprised of a ~20 nm top layer enriched with SiO_2 and a ~30 nm bottom layer enriched with PEI. In other words, the majority of the PEI chains were able to diffuse up to ~30 nm from the substrate surface, while fewer PEI chains diffused all the way up to the top surface. The SLD profile of the $[PEI(9.9)/SiO_2(4.7)]_2$ film shows a clear two-bilayer structure. The shape of the SLD profile for the first bilayer is quite similar to that of the $[PEI(9.9)/SiO_2(4.7)]_1$ film, except that the SLD values for the two regions are around 1×10^{-6} and 1.4×10^{-6} Å^{-2}, respectively. Both of these values are higher than those of the single bilayer film $[PEI(9.9)/SiO_2(4.7)]_1$, which suggests that more PEI chains from the first bilayer diffused out to the second bilayer to interact with upcoming SiO_2 nanoparticles during the deposition. To the best of our knowledge, this is the first report from neutron reflectometry that provides evidence for the diffusion of polymer chains during the e-LbL growth process.

It is worth noting that the total thicknesses of the $[PEI(9.9)/SiO_2(4.7)]_1$ and $[PEI(9.9)/SiO_2(4.7)]_2$ films deposited on silicon wafers are 53 and 170 nm, respectively. These thicknesses are well below those of the thin films deposited onto the SAM-modified QCM crystals, even though they clearly demonstrate the e-LbL growth. According to the QCM results (Figure 2 and Table 1), the $[PEI(9.9)/SiO_2(4.7)]_1$ and $[PEI(9.9)/SiO_2(4.7)]_2$ films grown on the SAM-modified quartz crystals are as thick as 82 and 352 nm, respectively. This vast difference in thickness is likely due to the substrate surface effect on the deposition of the first PEI layer. It is expected that it would be easier for the positively charged PEI chains to deposit onto the negatively charged SAM-modified QCM crystal surface than on the non-charged silicon wafer surface. Consequently, the number of PEI chains deposited during the first layer can significantly affect the subsequent assembly steps. This will be discussed in more detail in the following section.

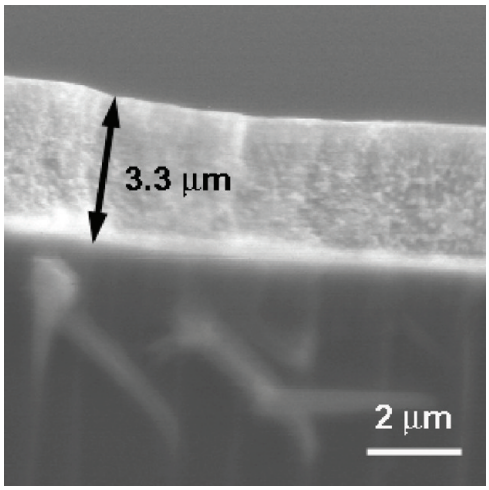

Figure 7. Cross-section SEM image of $[PEI(9.9)/SiO_2(4.7)]_{50}$ film grown on a glass substrate.

Explanation of the pH-Controlled e-LbL Growth. The vastly distinct assembly process and structure of the thin films when they were prepared at different pH values could be attributed to several reasons. One reason is the in-and-out diffusion of PEI chains toward the surface during the SiO_2 assembly step; another reason is the charge density variation of PEI chains at different pH values; and the third reason is the conformation change of PEI chains at different pH values. The proposed mechanism of film growth process, after the assembly of the first PEI and SiO_2 layer at different pH combinations, is illustrated in Figure 6. At the pH of 9.9, the majority of the amine groups of the PEI chains are deprotonated, and thus, the PEI chains have a low charge. As a result, a significant number of PEI chains are deposited onto the substrate to compensate for the surface charges, and the PEI chains form a collapsed structure on the substrate due to the low electrostatic repelling force between the chain segments (Figure 6a, left). During the subsequent SiO_2 assembly step, the collapsed PEI chains will extend as a result of the increased charge density of each PEI chain, and the excess PEI chains will diffuse out to the outer surface to interact with more SiO_2 nanoparticles. As a result, more than one monolayer of SiO_2 can be deposited during one single exponential growth step. Apparently, this exponential growth process will be significantly dependent on the charge density variation of every PEI chain. Therefore, when the pH difference between the PEI and SiO_2 solutions decreases, the exponential growth rate diminishes a lot (see Figure 2). Furthermore, when both the PEI and SiO_2 are assembled at the same pH of 4.7, the charge density and the conformation of PEI chains will not change between the PEI and SiO_2 deposition step (see Figure 6b). As a consequence, the $[PEI(4.7)/SiO_2(4.7)]_{10}$ film grows linearly (see Figure 2).

Further increasing the pH of the SiO_2 suspension to prepare the $[PEI(4.7)/SiO_2(9.5)]_{10}$ film will decrease the assembly rate even more as a result of the decreasing PEI charge from the PEI to the SiO_2 deposition step. In addition, because of the decreasing PEI charge from low to high pH, the initially extended PEI chains will collapse at the pH of 9.5 during the SiO_2 assembly step (see Figure 6c, left), and thus, the substrate surface cannot

dx.doi.org/10.1021/cm2019229 |Chem. Mater. 2011, 23, 4548–4556

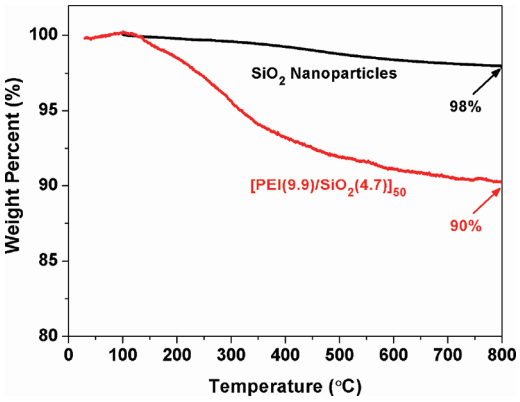

Figure 8. Thermogravimetric analysis of SiO_2 nanoparticles and the $[PEI(9.9)/SiO_2(4.7)]_{50}$ thin film.

be fully covered by the PEI chains. As a consequence, the negatively charged SiO_2 particles can only be deposited onto the few available positively charged surface sites on the substrate (see Figure 6c, right), and the film eventually grows into a clusterlike structure, which was observed in the AFM image presented in Figure 3d.

Inorganic Content of the e-LbL Films. To evaluate the inorganic content of the exponentially grown thin films, we prepared a 50-bilayer thin film $[PEI(9.9)/SiO_2(4.7)]_{50}$ on a glass substrate and studied its thickness and inorganic content using SEM and TGA. The SEM cross-sectional image in Figure 7 indicates that thin film $[PEI(9.9)/SiO_2(4.7)]_{50}$ is primarily composed of inorganic nanoparticles. The inorganic content of this thin film was further evaluated using TGA by heating the thin film and some colloidal SiO_2 particles separately up to 800 °C. As shown in Figure 8, about 90 wt % of the $[PEI(9.9)/SiO_2(4.7)]_{50}$ film is composed of noncombustible inorganic materials. In addition, the TGA analysis of the colloidal SiO_2 particles shows that 98 wt % of the colloidal particles are composed of noncombustible inorganic materials, and the other 2 wt % are combustible organic materials. Therefore, this means that more than 90% of the $[PEI(9.9)/SiO_2(4.7)]_{50}$ thin film is contributed by the colloidal SiO_2. To the authors' knowledge, this is the first time that such thick and dense films containing primarily inorganic nanoparticles have ever been manufactured using the LbL assembly method.

The thickness of film $[PEI(9.9)/SiO_2(4.7)]_{50}$ is around 3.3 μm according to the SEM image in Figure 7, which is less than what we would have expected from the QCM results (Figure 2 and Table 1). If the thin films grew at the same rate as that of the linear growth regime beyond the 10th layer, shown in the QCM results in Figure 2, the thickness of $[PEI(9.9)/SiO_2(4.7)]_{50}$ should have been around 8 μm. The difference can possibly be attributed to the fact that the thicker film was grown on glass rather than the SAM-modified quartz crystal, thus lowering the rate of growth as explained above, or the possibility that films begin cracking and particles begin to detach in the later assembly stages. It is not unreasonable to expect that this may happen when the majority of the thin film is composed of inorganic SiO_2 particles (see Figure S7 and Figure S8 in the Supporting Information). However, as it has been suggested that film cracking and particle detachment can be potentially eliminated by limiting the drying process during the assembly,[36] this should not be of too much concern for now.

In conclusion, the discovery of the pH-promoted e-LbL assembly of bicomponent PEI/SiO_2 thin films with high inorganic particle content provides the first step toward the fabrication of multifunctional films with designed properties. This feature will be very important for any type of film in which the inorganic interparticle connection is very critical for the film functionality or where specific gradients in density are desired.

CONCLUSIONS

A new type of exponentially grown organic/inorganic bicomponent composite thin film was demonstrated by the LbL assembly of PEI and SiO_2 nanoparticles. Our results show that the film growth rate is significantly dependent on the pH difference between the PEI and the SiO_2 solutions. Only when the thin film is deposited with PEI at a high pH and with SiO_2 at a low pH, will the thin film exhibit e-LbL growth. The exponential growth strength was shown to significantly decrease when this pH difference decreased or when the solutions had pH values in reverse. Introducing a pH buffer into the PEI and SiO_2 solution extends the exponential growth region somewhat and also increases the growth rate in the subsequent linear growth regime. Unlike the all-organic thin film systems reported by previous investigators, increasing the ionic strength of the PEI solution, in this case, eliminated the exponential growth, as a result of the strong screening effect of NaCl on the positive charges of the PEI chains.

In this work, the e-LbL $[PEI/SiO_2]_n$ grown thin films were primarily composed of inorganic SiO_2 nanoparticles. We were able to prepare thin films as thick as 2.1 μm composed of over 90% inorganic SiO_2 nanoparticles within 10 bilayers. To our knowledge, this is the first time a bicomponent polyelectrolyte/inorganic nanoparticle thin film with high inorganic content has been grown via e-LbL growth. The extremely fast thin film growth is attributed not only to the in-and-out diffusion of PEI chains but also to the PEI charge density increase when the pH is changed from a high to a low value. As a result of the diffusion of the PEI chains, e-LbL grown films exhibited a dual-scale structure with very smooth regions at a small scale (~2 μm) that form much rougher islands at a larger length scale (~30 μm). The fundamental understanding of the pH controlled e-LbL growth of organic/inorganic bicomponent thin films will have significant impact on the LbL assembly field.

ASSOCIATED CONTENT

Supporting Information. Information about the film thickness obtained using AFM and the effect of ionic strength and pH buffer on the e-LbL growth. Explanation for the surface roughness of 1−4 bilayer thin films and the thickness of the 50-bilayer thin film. This material is available free of charge via the Internet at http://pubs.acs.org.

AUTHOR INFORMATION

Corresponding Author
*E-mail: rosario.gerhardt@mse.gatech.edu.

ACKNOWLEDGMENT

This work was partially supported by U.S. Department of Energy Grant No. DE-FG-02-03-ER4603S and an Otto Kress Scholarship from the Institute of Paper Science and Technology at the Georgia Institute of Technology. Research at Oak Ridge National Laboratory's Spallation Neutron Source was sponsored

by the Scientific User Facilities Division, Office of Basic Energy Sciences, U.S. Department of Energy.

REFERENCES

(1) Iler, R. K. *J. Colloid Interface Sci.* **1966**, *21* (6), 569–594.
(2) Decher, G.; Hong, J. D.; Schmitt, J. *Thin Solid Films* **1992**, *210* (1−2), 831–835.
(3) Decher, G. *Science* **1997**, *277* (5330), 1232–1237.
(4) Jiang, C. Y.; Markutsya, S.; Pikus, Y.; Tsukruk, V. V. *Nat. Mater.* **2004**, *3* (10), 721–728.
(5) Lvov, Y.; Ariga, K.; Onda, M.; Ichinose, I.; Kunitake, T. *Langmuir* **1997**, *13* (23), 6195–6203.
(6) Park, J.; Fouche, L. D.; Hammond, P. T. *Adv. Mater.* **2005**, *17* (21), 2575–2579.
(7) Tang, Z. Y.; Kotov, N. A.; Magonov, S.; Ozturk, B. *Nat. Mater.* **2003**, *2* (6), 413–418.
(8) Podsiadlo, P.; Kaushik, A. K.; Arruda, E. M.; Waas, A. M.; Shim, B. S.; Xu, J. D.; Nandivada, H.; Pumplin, B. G.; Lahann, J.; Ramamoorthy, A.; Kotov, N. A. *Science* **2007**, *318*, 80–83.
(9) Lee, S. W.; Kim, B. S.; Chen, S.; Shao-Horn, Y.; Hammond, P. T. *J. Am. Chem. Soc.* **2009**, *131* (2), 671–679.
(10) Chang, S. H.; Ko, H. H.; Singamaneni, S.; Gunawidjaja, R.; Tsukruk, V. V. *Anal. Chem.* **2009**, *81* (14), 5740–5748.
(11) Jiang, C. Y.; Lio, W. Y.; Tsukruk, V. V. *Phys. Rev. Lett.* **2005**, *95*, 115503.
(12) Srivastava, S.; Kotov, N. A. *Acc. Chem. Res.* **2008**, *41* (12), 1831–1841.
(13) Jaffar, S.; Nam, K. T.; Khademhosseini, A.; Xing, J.; Langer, R. S.; Belcher, A. M. *Nano Lett.* **2004**, *4* (8), 1421–1425.
(14) Shi, F.; Wang, Z. Q.; Zhao, N.; Zhang, X. *Langmuir* **2005**, *21* (4), 1599–1602.
(15) Lvov, Y.; Ariga, K.; Kunitake, T. *Chem. Lett.* **1994**, *23* (12), 2323–2326.
(16) Yoo, P. J.; Nam, K. T.; Qi, J. F.; Lee, S. K.; Park, J.; Belcher, A. M.; Hammond, P. T. *Nat. Mater.* **2006**, *5* (3), 234–240.
(17) Elbert, D. L.; Herbert, C. B.; Hubbell, J. A. *Langmuir* **1999**, *15* (16), 5355–5362.
(18) Picart, C.; Lavalle, P.; Hubert, P.; Cuisinier, F. J. G.; Decher, G.; Schaaf, P.; Voegel, J. C. *Langmuir* **2001**, *17* (23), 7414–7424.
(19) Picart, C.; Mutterer, J.; Richert, L.; Luo, Y.; Prestwich, G. D.; Schaaf, P.; Voegel, J. C.; Lavalle, P. *Proc. Natl. Acad. Sci. U.S.A.* **2002**, *99* (20), 12531–12535.
(20) Lavalle, P.; Gergely, C.; Cuisinier, F. J. G.; Decher, G.; Schaaf, P.; Voegel, J. C.; Picart, C. *Macromolecules* **2002**, *35* (11), 4458–4465.
(21) Richert, L.; Lavalle, P.; Payan, E.; Shu, X. Z.; Prestwich, G. D.; Stoltz, J. F.; Schaaf, P.; Voegel, J. C.; Picart, C. *Langmuir* **2004**, *20* (2), 448–458.
(22) Liu, X. K.; Zhou, L.; Liu, F.; Ji, M. Y.; Tang, W. G.; Pang, M. J.; Sun, J. Q. *J. Mater. Chem.* **2010**, *20* (36), 7721–7727.
(23) Schmidt, D. J.; Moskowitz, J. S.; Hammond, P. T. *Chem. Mater.* **2010**, *22* (23), 6416–6425.
(24) Kujawa, P.; Moraille, P.; Sanchez, J.; Badia, A.; Winnik, F. M. *J. Am. Chem. Soc.* **2005**, *127* (25), 9224–9234.
(25) Pardo-Yissar, V.; Katz, E.; Lioubashevski, O.; Willner, I. *Langmuir* **2001**, *17* (4), 1110–1118.
(26) McAloney, R. A.; Sinyor, M.; Dudnik, V.; Goh, M. C. *Langmuir* **2001**, *17* (21), 6655–6663.
(27) Salomaki, M.; Vinokurov, I. A.; Kankare, J. *Langmuir* **2005**, *21* (24), 11232–11240.
(28) Fu, J. H.; Ji, J.; Shen, L. Y.; Kueller, A.; Rosenhahn, A.; Shen, J. C.; Grunze, M. *Langmuir* **2009**, *25* (2), 672–675.
(29) Laugel, N.; Betscha, C.; Winterhalter, M.; Voegel, J. C.; Schaaf, P.; Ball, V. *J. Phys. Chem. B* **2006**, *110* (39), 19443–19449.
(30) Peng, C. Q.; Thio, Y. S.; Gerhardt, R. A. *Nanotechnology* **2008**, *19* (50), 505603.
(31) Peng, C. Q.; Thio, Y. S.; Gerhardt, R. A. *J. Phys. Chem. C* **2010**, *114* (14), 9685–9692.
(32) Park, Y. T.; Ham, A. Y.; Grunlan, J. C. *J. Phys. Chem. C* **2010**, *114* (14), 6325–6333.
(33) Lvov, Y.; Ariga, K.; Ichinose, I.; Kunitake, T. *J. Am. Chem. Soc.* **1995**, *117* (22), 6117–6123.
(34) Laugel, N.; Hemmerle, J.; Porcel, C.; Voegel, J. C.; Schaaf, P.; Ball, V. *Langmuir* **2007**, *23*, 3706–3711.
(35) Zouari, R.; Michel, M.; Di Martino, J.; Ball, V. *Mater. Sci. Eng., C: Matter. Biol. Appl.* **2010**, *30*, 3706.
(36) Podsiadlo, P.; Michel, M.; Lee, J.; Verploegen, E.; Kam, N. W. S.; Ball, V.; Qi, Y.; Hart, A. J.; Hammond, P. T.; Kotov, N. A. *Nano Lett.* **2008**, *8* (6), 1762–1770.
(37) Podsiadlo, P.; Michel, M.; Critchley, K.; Srivastava, S.; Qin, M.; Lee, J. W.; Verploegen, E.; Hart, A. J.; Qi, Y.; Kotov, N. A. *Angew. Chem., Int. Ed.* **2009**, *48* (38), 7073–7077.
(38) Meszaros, R.; Thompson, L.; Bos, M.; de Groot, P. *Langmuir* **2002**, *18* (16), 6164–6169.
(39) Smith, M. *March's Advanced Organic Chemistry: Reactions, Mechanisms, and Structure*, 6th ed.; Wiley-Interscience: Hoboken, NJ, 2007; pp 359−364.
(40) Shepherd, E. J.; Kitchener, J. A. *J. Chem. Soc.* **1956**, 2448–2453.
(41) Sauerbrey, G. *Z. Phys. Chem.* **1959**, 206–222.
(42) Lauter, V.; Ambaye, H.; Goyette, R.; Lee, W. T. H.; Parizzi, A. *Physica B* **2009**, *404*, 2543–2546.
(43) *Instrument 4A Fact Sheet*; Oak Ridge National Laboratory: Oak Ridge, TN, 2011; www.sns.gov/instruments/SNS/factsheets/Instrument_4a.pdf .
(44) Porcel, C.; Lavalle, P.; Ball, V.; Decher, G.; Senger, B.; Voegel, J. C.; Schaaf, P. *Langmuir* **2006**, *22*, 4376–4383.
(45) Porcel, C.; Lavalle, P.; Decher, G.; Senger, B.; Schaaf, P. *Langmuir* **2007**, *23*, 1898–1904.
(46) Hubsch, E.; Ball, V.; Senger, B.; Decher, G.; Voegel, J. C.; Schaaf, P. *Langmuir* **2004**, *20*, 1980–1985.
(47) Evans, D. F.*The Colloidal Domain: Where Physics, Chemistry, Biology, and Technology Meet*, 2nd ed.; Wiley-VCH: New York, 1999.
(48) Boulmedais, F.; Ball, V.; Schwinte, P.; Frisch, B.; Schaaf, P.; Voegel, J. C. *Langmuir* **2003**, *19*, 440–445.
(49) Penfold, J.; Thomas, R. K. *J. Phys.—Condens. Matter* **1990**, *2*, 1369–1412.